Chemical Science

EDGE ARTICLE

CrossMark
click for updates

Stabilization of volatile Ti(BH$_4$)$_3$ by nano-confinement in a metal–organic framework†

E. Callini,*[ab] P. Á. Szilágyi,[cd] M. Paskevicius,[de] N. P. Stadie,[b] J. Réhault,[f] C. E. Buckley,[d] A. Borgschulte[bg] and A. Züttel[ab]

Liquid complex hydrides are a new class of hydrogen storage materials with several advantages over solid hydrides, *e.g.* they are flexible in shape, they are a flowing fluid and their convective properties facilitate heat transport. The physical and chemical properties of a gaseous hydride change when the molecules are adsorbed on a material with a large specific surface area, due to the interaction of the adsorbate with the surface of the host material and the reduced number of collisions between the hydride molecules. In this paper we report the synthesis and stabilization of gaseous Ti(BH$_4$)$_3$. The compound was successfully stabilized through adsorption in nanocavities. Ti(BH$_4$)$_3$, upon synthesis in its pure form, spontaneously and rapidly decomposes into diborane and titanium hydride at room temperature in an inert gas, *e.g.* argon. Ti(BH$_4$)$_3$ adsorbed in the cavities of a metal organic framework is stable for several months at ambient temperature and remains stable up to 350 K under vacuum. The adsorbed Ti(BH$_4$)$_3$ reaches approximately twice the density of the gas phase. The specific surface area (BET, N$_2$ adsorption) of the MOF decreased from 1200 m^2 g^{-1} to 770 m^2 g^{-1} upon Ti(BH$_4$)$_3$ adsorption.

Introduction

Materials for energy storage and conversion are key elements that drive the evolution of the energy landscape. Energy efficiency strategies of existing processes and solutions for energy-storage challenges[1] are being intensely investigated. However, sustainable solutions may only be implemented if conventional fossil-based energy sources are replaced with renewable energy fluxes. The intermittency of these fluxes implies that the reversible storage of energy carriers is fundamental for a realistic and reliable alternative to the fossil-fuel-based society.[2]

Because of its energy density (142 MJ kg^{-1}), hydrogen has been widely studied as a potential energy vector that could enable the transition to renewable energy sources.[2] While the

economic and technological challenges of the entire hydrogen cycle have been addressed, including its production, detection, and delivery, hydrogen storage with a high gravimetric and volumetric hydrogen density has remained one of the main challenges for the implementation of a hydrogen-based economy. The storage of hydrogen in the form of metal or complex hydrides exhibits very high volumetric hydrogen densities up to twice the density of liquid hydrogen.[3] MgH$_2$,[4,5] LiBH$_4$ (ref. 6 and 7) and Mg(BH$_4$)$_2$ (ref. 8 and 9) have been intensively studied as storage materials. However, most of these high hydrogen density solid compounds are too stable to spontaneously release hydrogen close to ambient conditions. Instead, they release hydrogen at conditions that do not match the requirements for practical applications, for instance, in combination with proton-exchange membrane (PEM) fuel-cell technology.[10,11] An alternative approach is to use less stable hydrides that are gaseous or liquid under ambient conditions.[12,13] The advantage of having a spontaneous hydrogen emitting reaction at room temperature is counteracted by the practical problems of handling such compounds. For example, Ti(BH$_4$)$_3$ and Al(BH$_4$)$_3$ spontaneously decompose into hydrogen and other products within hours, minutes or seconds[14,15] and are highly flammable in contact with air.

Inspired by the confinement of acetylene molecules in microporous materials,[16] several successful attempts to stabilize unstable complex hydrides have been achieved *via* matrix encapsulation or inorganic complexing.[17–19] The drawback of these previous investigations is that irreversible chemical reactions between the matrix and the complexes with the

[a] EPFL, Swiss Federal Institute of Technology, Laboratory of Materials for Renewable Energy, Rue de l'Industrie 17, 1950 Sion, Switzerland. E-mail: elsa.callini@epfl.ch

[b] Empa, Swiss Federal Laboratories for Materials Science and Technology, Laboratory 505 Hydrogen & Energy, Überlandstrasse 129, 8600 Dübendorf, Switzerland

[c] University of Greenwich, Central Avenue, Medway Campus, Chatham Maritime ME4 4TB, UK

[d] Department of Physics, Astronomy and Medical Radiation Sciences, Curtin University, GPO Box U1987, Perth, WA 6845, Australia

[e] Department of Chemistry & iNANO, Aarhus University, Langelandsgade 140, Aarhus 8000, Denmark

[f] Paul Scherrer Institute, PSI, CH-5232 Villigen, Switzerland

[g] Empa, Swiss Federal Laboratories for Materials Science and Technology, Laboratory 502 Advanced Analytical Technologies, Überlandstrasse 129, 8600 Dübendorf, Switzerland

† Electronic supplementary information (ESI) available: Structural characterizations and fit parameters. See DOI: 10.1039/c5sc03517a

hydrides inhibit the reversible use of the matrix and change the decomposition reaction pathway of the hydrides. In addition, their use of catalysts and/or structural modifications may lead to the formation of transient states during stabilization, which are difficult to detect. Rapidly evolving species (RES) is a general term that describes thermodynamically unstable phases evolving from chemical reactions that spontaneously react/transform on a short timescale. To determine the mechanisms of multi-step reactions, the role of the involved intermediates or transient species must be clarified. Examples of reactions where the formation of transient or intermediate species can alter the overall process include the adsorption of molecules on a surface[20] or catalytic processes, such as gas conversion and reduction.[21–24] Structural and thermodynamic information is indispensable for controlling and engineering reaction pathways, which is a crucial issue for reliable and safe energy conversion and storage.

In this work, we investigate the stabilization of a gaseous RES *via* physisorption in the nanocavities of a metal–organic framework (MOF), as schematically shown in Fig. 1. The MOF contains and stabilizes the gaseous molecules, and the RES shows no structural changes over months. Moreover, the eventual decomposition reaction pathway is dramatically changed, underlining the fact that a thermodynamic alteration has occurred.

$Ti(BH_4)_3$ was selected as the gas molecule for this study because of its interesting properties for energy storage (containing 13 wt% hydrogen). It is a highly unstable gas under ambient conditions and can be obtained as the metathesis product of $LiBH_4$ and $TiCl_3$.[13] In this synthetic approach, nitrogen flow carried newly synthesized $Ti(BH_4)_3$ molecules from the reactor to a cold trap containing the adsorbent MOF, UiO-66 (ref. 25 and 26) (see Methods). The zirconium-based MOF UiO-66 was chosen due to its exceptional thermal stability (up to 770 K),[27] the suitability of its cage size (1.6–1.7 nm diameter)[27] for confining the $Ti(BH_4)_3$ molecules, and its white color, which facilitates the detection of any color changes due to guest additions. The exploitation of porous materials experienced a breakthrough in the past decade, once the properties of metal–organic frameworks as adsorbents were discovered.[28–32] The major effort to date has been in finding materials with an increased gas storage capacity and/or selectivity.[33–37] However, the peculiarity of the present case lies in the fact that the adsorbed molecule is thermodynamically unstable; therefore, the strategic goal is controlling its rapid decomposition.
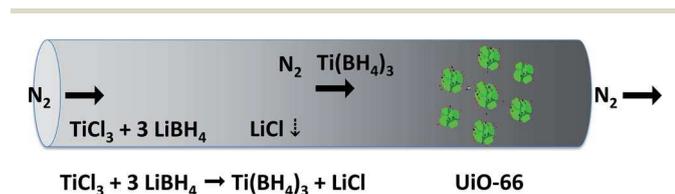
Experimental

All chemicals were purchased from Sigma Aldrich and were used without further purification.

UiO-66 ($Zr_6O_4(BDC)_6$, BDC = 1,4-benzenedicarboxylate) was prepared using the facile synthetic route developed by Farha *et al.*[26] First, 123 mg of 1,4-benzenedicarboxylic acid was mixed with 125 mg of $ZrCl_4$, 1 cm^3 of hydrochloric acid and 15 cm^3 of dimethyl formamide (DMF) in a scintillation vial. The reaction mixture was allowed to react at 350 K overnight. The product was filtered, and the remaining unreacted reagents were removed while the high-boiling point DMF was exchanged to tetrahydrofuran (THF) overnight at 430 K using a Soxhlet apparatus. Prior to further use, UiO-66 was activated for 16 h under vacuum at 490 K.

$Ti(BH_4)_3$ was produced by the metathesis between $LiBH_4$ and $TiCl_3$ (3 : 1 molar ratio) *via* ball milling for 10 minutes in a PQ-N04 planetary mill (Across International) using a stainless steel vial (100 mL) and stainless steel balls (diameter: 10 mm). It was then captured in UiO-66 within a cold trap at 200 K. First, the cold trap was filled with UiO-66 in an Ar glovebox to avoid exposure to air. Then, the trap was sealed and allowed to cool in a dry-ice–acetone bath to *ca.* 200 K under a constant N_2 flow (1.5 bar). After milling, the reaction mixture was inserted into a flow reactor at room temperature, and the nitrogen flow was allowed to carry the gaseous $Ti(BH_4)_3$ from the reactor to the trap, enabling gas adsorption on the MOF surface. To separate unwanted volatile side products (*e.g.* diborane), we made use of the differences in their boiling points (T_b diborane = 181 K, whereas $Ti(BH_4)_3$ is in a condensed state at 200 K); thus, the dry ice cold trap allowed for the selective condensation of the desired product. The $Ti(BH_4)_3$-loaded UiO-66 was then kept at room temperature and pressure in a glove box for further investigations.

X-ray diffraction (XRD) data were collected in the Bragg–Brentano geometry using a Bruker D8 Advance diffractometer (CuKα radiation). Samples were loaded into XRD low background (Si single crystal) sample holders in an argon glove box and sealed within a poly(methylmethacrylate) (PMMA) air-tight holder to prevent oxygen/moisture contamination during data collection.

The chemical composition of the $Ti(BH_4)_3$-loaded UiO-66 was verified by probing the Ti : Zr ratio using energy-dispersive X-ray spectroscopy (EDX) using a Zeiss EVO 40 XVP scanning electron microscope equipped with an Oxford Instruments energy dispersive X-ray spectrometer (EDS) at an accelerating voltage of 20 kV. The samples were briefly (<1 min) exposed to air and were not coated prior to measurement.

Equilibrium N_2 adsorption isotherms at 77 K were acquired for the activated samples, using a Micromeritics Tristar II 3020 instrument, measuring 20 data points during both adsorption and desorption. The Brunauer–Emmett–Teller surface areas were calculated with the help of the Micromeritics software package and using the linear region of the adsorption isotherms (data points up to 0.2 p p$_0^{-1}$). Barrett–Joyner–Halenda pore size

Fig. 1 Schematic representation of gas adsorption by a MOF. The gas molecules ($Ti(BH_4)_3$) were synthesized in a reactor and adsorbed on the MOF (UiO-66) under N_2 flow.

and volume analysis was performed using the Micromeritics software package.

Raman spectra were acquired using a WITec alpha 300SAR confocal Raman microscopy system (WITec GmbH, Ulm Germany). All Raman measurements were performed using a frequency-doubled Nd:YAG laser with an excitation wavelength of 532 nm and the $100\times$ objective of the confocal microscope (Zeiss EC "Epiplan-Neofluar" $100\times$ NA $= 0.9$; WD $= 0.31$ mm). In total, 10–1000 spectra were acquired with an integration time of *ca.* 80 ms. The spectral resolution of this instrument is ± 3 cm^{-1}. The spectra were corrected using the built-in background subtraction function of the system.

Decomposition of Ti(BH$_4$)$_3$ was monitored with the aid of a temperature-programmed sealed autoclave coupled to a mass spectrometer (TPD-MS), which allowed for the detection of volatile species. Mass spectra were collected using a Stanford Research Systems (SRS) residual gas analyzer (RGA 300) quadrupole mass spectrometer. The Ti(BH$_4$)$_3$-loaded UiO-66 was placed in a sealed AISI316 VCR sample holder, outgassed at 3×10^{-7} bar and 300 K overnight. While still under vacuum, the samples were heated to 460 K at a heating rate of 0.5 K min^{-1}. The evolved gases were constantly monitored from 1 to 100 atomic mass units (AMU).

Multivariate curve resolution (MCR) is a method for analysing the evolution of spectral peaks. In this case, the analysis is applied to the temperature evolution of the MS spectra. The matrix of the MS spectra is expressed as the product of a fixed number of simulated spectra and their concentrations. Each of the simulated spectra represents the emission of a specific group of species. For the analysis, the MATLAB software package was used, adopting the so-called MCR-ALS script.[43,44] In this case, the best fit of the MS data was achieved using 2 simulated spectra, which means that the reaction has two steps, each of which is associated with the emission of specific fragments. The result of the fit gives the concentration of the two simulated spectra as a function of the temperature and, thus, the temperature evolution of the associated species.

Results

Adsorption of thermodynamically unstable gas molecules on MOF nanocavities

Various methods were used to confirm the successful incorporation of Ti(BH$_4$)$_3$ into the porous structure of the MOF. Complete reaction of the starting materials to produce Ti(BH$_4$)$_3$ was verified using X-ray diffraction (XRD) of the residue powder in the reactor, showing that LiCl was the only crystalline phase after the metathesis reaction, as previously reported[13] (ESI Fig. S1†). Visibly, the MOF powder underwent a white-to-grey color change upon exposure to gaseous Ti(BH$_4$)$_3$ (ESI Fig. S2†). Energy-dispersive X-ray (EDX) spectroscopy of the loaded MOF revealed the presence of Ti (ESI Fig. S3†), which is not present in the MOF pre-exposure. The Brunauer–Emmett–Teller (BET) surface area of the loaded MOF, determined using nitrogen adsorption at 77 K, was found to be roughly half that of the pristine MOF prior to loading: 770 m^2 g^{-1} (ESI Fig. S4†). The Barrett–Joyner–Halenda (BJH) pore-size analysis,[38] probing the

variation of the average pore diameter of UiO-66 after the addition of Ti(BH$_4$)$_3$, revealed a decrease in the average pore width after loading of 3.44 Å (ESI Table S1†).

Most importantly, the incorporation of Ti(BH$_4$)$_3$ into the pores of the MOF was unambiguously demonstrated using solid-state Raman spectroscopy of the loaded material. The vibrational modes appearing in the 2400–2550 cm^{-1} range correspond to the B–H stretching mode of the BH$_4$ unit in Ti(BH$_4$)$_3$, in agreement with previous observations of solid complex hydrides.[39] The intensity of the B–H stretching mode at 2435 cm^{-1} is approximately 10% of the primary MOF mode at 1611 cm^{-1}, giving a qualitative indication of the success of the gas adsorption. Fig. 2 shows the Lorentzian fitted Raman spectrum at room temperature of the as-prepared UiO-66 (spectrum a) and the same material after exposure to Ti(BH$_4$)$_3$ gas (spectrum b), where the B–H stretching modes are evident, in the region between 2400–2550 cm^{-1}; the raw data and fit parameters are given in the ESI Fig. S5.† The vibrational modes of UiO-66 are present in all spectra. The modes between 650 and 1700 cm^{-1} can be attributed to organic linkers.[40–42] These modes are not significantly altered upon Ti(BH$_4$)$_3$ adsorption (within the instrumental spectral resolution of ± 3 cm^{-1}), likely due to their much larger number compared to the adsorbed molecules in this work.

The adsorbed Ti(BH$_4$)$_3$ is stable over time, when kept in an argon glove box at ambient pressure and temperature. Raman spectroscopy of the Ti(BH$_4$)$_3$ – exposed material after several months demonstrated that the stabilized gas remained adsorbed in the nanocavities of the MOF, as shown in Fig. 2. This implies that a remarkable increase in stability was achieved, since pure Ti(BH$_4$)$_3$ decomposes in less than a few hours under an argon atmosphere at ambient pressure and temperature.[13]
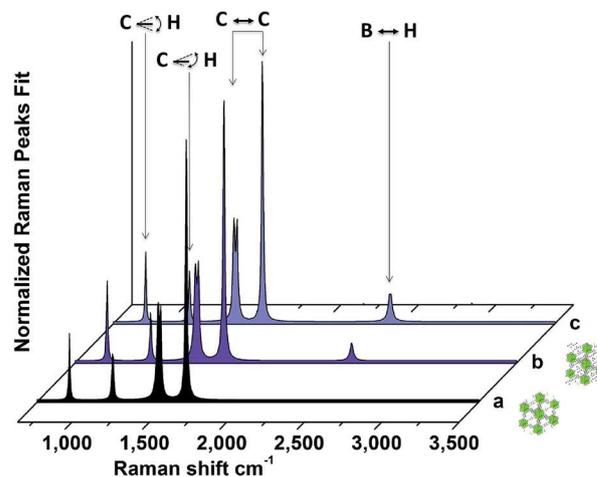

Fig. 2 Fitted Raman spectra showing successful gas adsorption on the MOF and the stabilization of the gas molecule. Fitted Raman spectra at room temperature for (a) the pristine MOF, (b) the loaded MOF and (c) the loaded MOF after 1 month in an argon atmosphere at ambient pressure and room temperature. The illustrations represent the pristine and loaded MOF. The vibrations are assigned as follows: 650–900 cm^{-1} C–H out-of-plane bending; 1140 cm^{-1} C–H in-plane bending; 1430–1625 cm^{-1} C–C stretching; 2435 cm^{-1} B–H stretching, visible only in the loaded sample.[40]

Stabilization of the thermodynamically unstable gas molecules

The incorporation of $Ti(BH_4)_3$ into the nanocavities of the MOF not only stabilizes the borohydride with respect to time, as discussed above, but also makes it more thermally stable. The mechanism of the adsorbed complex hydride decomposition was investigated using temperature-programmed desorption combined with mass spectrometry (TPD-MS) and Raman spectroscopy (Fig. 3 and 4, respectively). The loaded MOF was heated under vacuum ($<10^{-3}$ mbar), and the mass spectra of the evolved gases were acquired as a function of the temperature of the sample, as shown in Fig. 3b. Unlike in the case of pure $Ti(BH_4)_3$ decomposition,[13] no signal from diborane was detected at room temperature. The mass-to-charge (m/z) signals from Ti–B–H containing fragments appear near 350 K. B–H fragments (BH_4 $m/z = 15$; $(BH_4)_2$ $m/z = 30$; $(BH_4)_3$ $m/z = 45$ or B_5H_9 $m/z = 58, 59$) and Ti containing species ($Ti^{10,11}B_2H_4$ $m/z = 72$, 73 and $Ti^{10,11}B_3H_{10}$ $m/z = 90, 91$) are discernible, which is a distinctly different behavior from that which was previously

observed for the decomposition of pure $Ti(BH_4)_3$ either under ultra-high vacuum or at ambient pressure, both of which yielded diborane as the main decomposition product at room temperature.[13] To correlate and identify the formation of the intermediate species during the decomposition of $Ti(BH_4)_3$, multivariate curve resolution (MCR) analysis was performed on the TPD-MS data.[43,44] The results of the analysis are shown in Fig. 3a and c, where the matrix of the TPD-MS spectra is expressed as the product of a fixed number of calculated spectra (Fig. 3a) multiplied by their concentrations (Fig. 3c). TPD-MS data are best fitted with two simulated spectra (percent of variance at the optimum = 99.5659), which differ mainly in the 55–65 and 90–95 m/z regions (Fig. 3a). The plot of the concentrations of the simulated spectra as a function of the temperature (Fig. 3c) reveals a two-step process. No emission of species was detectable below 350 K apart from impurities. The black curve in Fig. 3c represents the emission of the intermediate species (such as B_5H_9) that disappear at approximately 410 K. The red curve represents the continuous emission of species (e.g., B–H units) up to 430 K, when the sample is completely
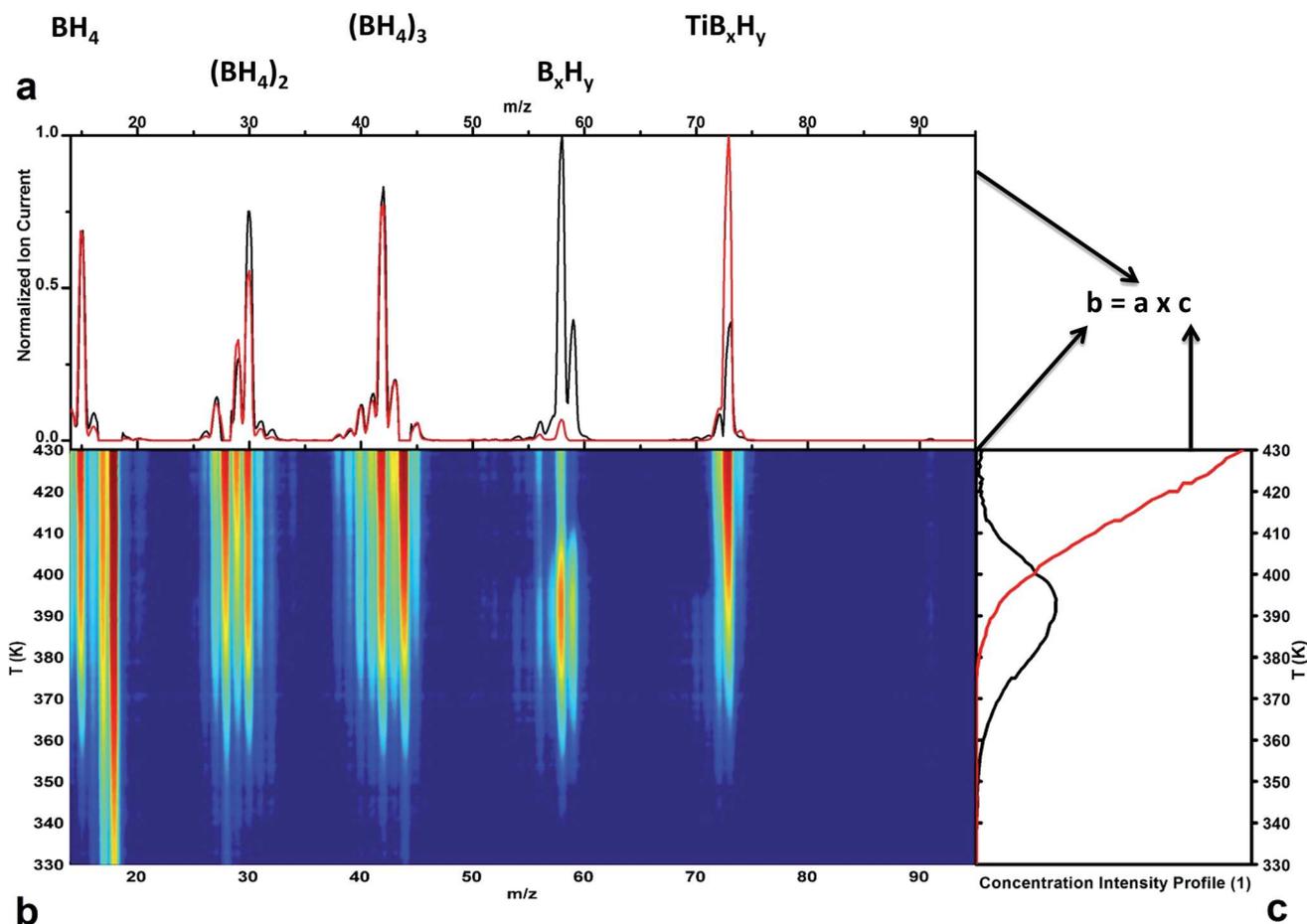

Fig. 3 TPD-MS, Raman spectroscopy and MCR analysis showing the decomposition reaction of the adsorbed gas molecules from the MOF. The TPD-MS matrix (panel b) is expressed as the product of the simulated spectra (panel a) and their concentrations (panel c). In detail, panel a: simulated TPD-MS spectra from the MCR analysis (impurities have been removed from the input data). The experimental data in panel b were best fitted with two simulated spectra (black and red curves). Panel b: experimental TPD-MS spectra of the adsorbed sample during the heating ramp. The intensities of the signals in arbitrary units are represented by a range of colors from blue (ion current = min) to red (ion current = max). Panel c: concentration profiles of the simulated TPD-MS spectra in panel a[43,44] as a function of the temperature from the MCR analysis.
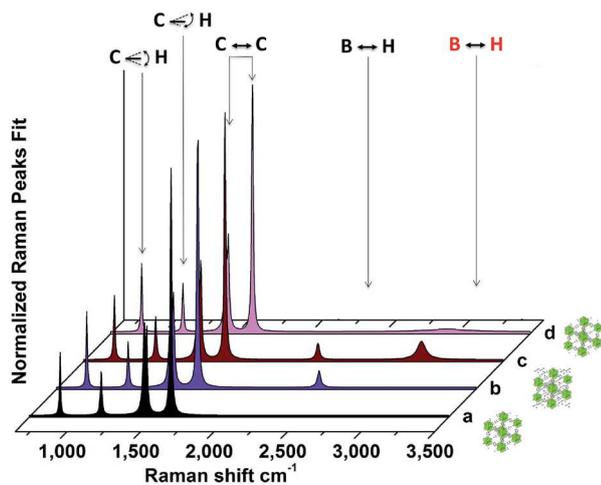
Fig. 4 Fitted Raman spectra showing the decomposition of the loaded MOF. Fitted Raman spectra at room temperature for (a) the pristine MOF, (b) the loaded MOF, (c) the loaded MOF after heating in a vacuum to 470 K, and (d) the loaded MOF after TPD-MS and air exposure. The illustrations represent the loaded and pristine MOF. The vibrations are assigned as follows: $650-900$ cm^{-1} C–H out-of-plane bending; 1140 cm^{-1} C–H in-plane bending; $1430-1625$ cm^{-1} C–C stretching; 2435 cm^{-1} B–H stretching, visible only in the loaded sample;[40] 2245 and 2950 cm^{-1} B–H stretching, visible only in the sample after heat treatment.

decomposed. This result suggests that the decomposition of the adsorbed Ti(BH$_4$)$_3$ proceeds *via* an intermediate step.

To better characterize these decomposition products, *ex situ* Raman spectra of the loaded MOF were acquired at room temperature after the TPD-MS treatment. Fig. 4 shows the Lorentzian fitted Raman spectrum of UiO-66 in its as-prepared form (spectrum a), after Ti(BH$_4$)$_3$ gas exposure (spectrum b), and after TPD-MS treatment up to 470 K and cooling back to room temperature (spectrum c). In the post-decomposition MOF sample (spectrum c), the B–H stretching mode at 2435 cm^{-1} disappears, and two modes at 2245 and 2950 cm^{-1} appear. The high energy of the latter mode could correspond to transient C–H interactions; however, there is no further indication of changes in the MOF structure, *i.e.*, in the C–H bending region. Both modes might be assigned to B–H stretching modes of the intermediate species and products from the evolution of the BH$_4$ unit. The B–H bond can stretch and shift its characteristic vibration frequencies upon distortion of the BH$_4$ unit, as previously demonstrated by Raman spectroscopy studies of borohydrides.[45] Raw data and the fit parameters are given in the ESI, Fig. S6.†

The additional modes observed in the Raman spectrum of the loaded MOF after decomposition of the adsorbed Ti(BH$_4$)$_3$ disappear upon prolonged laser irradiation or air exposure (Fig. 4 spectrum d). The fully decomposed spectrum is identical to that of the pristine MOF (comparing Fig. 4 spectrum d to Fig. 4 spectrum a). No B–H stretching modes remain, and the Raman modes corresponding to the pristine MOF do not present any apparent changes (complete raw data and fit parameters are given in the ESI, Fig. S6†), indicating that the

MOF did not undergo any structural changes upon guest adsorption and release. XRD measurements (ESI Fig. S7†) of the MOF before and after guest adsorption reveal that no significant structural changes have occurred in the specimen. While chemisorption of Ti(BH$_4$)$_3$ on UiO-66 may occur to some extent, our experimental data strongly suggest that the framework remained intact upon guest sorption. Visibly, the MOF reverts to its original white color after decomposition of Ti(BH$_4$)$_3$, or after the release of the adsorbed gas to air.

Discussion

The presented data show several results: Ti(BH$_4$)$_3$ is incorporated into the MOF, the loaded sample is stable over time if kept in an inert atmosphere (argon, 1 bar, room temperature), and Ti(BH$_4$)$_3$ is released and decomposes at 350 K without diborane emission. The gaseous Ti(BH$_4$)$_3$ molecule is normally thermodynamically unstable. Therefore, the adsorption of Ti(BH$_4$)$_3$ on the MOF alters the stability of the Ti(BH$_4$)$_3$ and enables the characterization of the normally transient species. To interpret this stabilization, we seek its origin in the host–guest interaction.

The molecule of Ti(BH$_4$)$_3$ decomposes spontaneously at room temperature. This process is favored by collisions with surface phonons, photons or other Ti(BH$_4$)$_3$ molecules. In the loaded MOF, the encapsulated Ti(BH$_4$)$_3$ molecules can diffuse and migrate within the porous structure. However, intermolecular collisions are hindered when the gas molecules are highly dispersed and thus diluted on the supporting framework. When this is the case, the Ti(BH$_4$)$_3$ molecules are held at a certain distance from one another, and their stabilization would then be achieved by restricting the reactions between two molecules, as for acetylene.[16] This behavior would imply that, on average, each Ti(BH$_4$)$_3$ molecule is confined in a pore. When a guest is adsorbed in the pores of a scaffold, the pore size decreases accordingly; indeed we observed a decrease in the average pore width after loading of 3.44 Å. Because the narrowest diameter of the non-spherical Ti(BH$_4$)$_3$ molecules is approximately 2 Å,[46] it is therefore suggested that, on average, there is more than one Ti(BH$_4$)$_3$ molecule per UiO-66 pore, which means that the guest molecules are close enough to replicate the phase-pure reaction and that their stabilization is not due to the dilution of the molecules. This result is supported by the rough estimation of Ti(BH$_4$)$_3$ loading in the MOF, as suggested by Raman spectroscopy shown in Fig. 2. By taking into account such a successful loading process, the Ti(BH$_4$)$_3$ molecules should be able to migrate and react as they would outside of the MOF, unless they were adsorbed onto the surfaces of the MOF pores.

If Ti(BH$_4$)$_3$ was adsorbed to the pore surface of the MOF, the molecule's potential would be altered due to the strong host–guest bonds, which is confirmed by Raman spectroscopy. Previous spectroscopic studies on pure gaseous Ti(BH$_4$)$_3$ exhibit two distinct peaks in the B–H stretching range.[13] The splitting of the B–H stretching modes is due to the highly asymmetrical configuration of the BH$_4$ units, which have three hydrogen atoms (H$_b$) bridged between the titanium and boron and one

terminal hydrogen atom (H_t) bonded uniquely to the boron (tridental configuration). Infrared spectroscopy of Ti(BH$_4$)$_3$ molecules in the gas phase reveals a mode at 2025 cm^{-1} that is assignable to the B–H$_b$ vibration and a mode at 2590 cm^{-1} that is assignable to the B–H$_t$ vibration.[13,47] Due to the C_{3h} symmetry of the Ti(BH$_4$)$_3$ molecule,[47] these vibrations are also Raman active and therefore should be present in the spectra of the loaded sample. Conversely, in Fig. 2, the single B–H stretching peak at 2435 cm^{-1} suggests a symmetrical configuration of the [BH$_4$]$^-$ ion, typical of stable complex hydrides.[7,45] The shift of the B–H$_b$ stretching mode to 17% higher energy reflects a change in the binding energy of the B–H atoms.[48] The bond dissociation energy in diatomic B–H is 3.5 eV; therefore, a stabilization of 0.6 eV is achieved. This stabilized system should induce a shift in the decomposition temperature of approximately 67 K. Gaseous Ti(BH$_4$)$_3$ molecules decompose at room temperature,[13] while, as shown in Fig. 3 by mass spectroscopy, the loaded sample does not decompose below 350 K: approximately 57 K above room temperature and in agreement with the calculation on the stabilization of the molecule.

The lack of Ti(BH$_4$)$_3$ bending modes in the Raman spectrum of the loaded MOF supports the hypothesis of a change in the symmetry of the molecule. In addition, when a molecule is adsorbed on a substrate, the selection rules for Raman activity differ from the ones for the free molecule.[49] The surface–gas interaction also explains the stabilization effect of the MOF on the Ti(BH$_4$)$_3$ molecule: the MOF surface lowers the free energy of the molecule. A similar effect has been observed for microporous siliceous frameworks.[50] The adsorption of transition states or RES on these surfaces is favored even in the absence of specific sites for chemical binding. It may therefore be possible that, as a general rule, the physisorption of transient or thermodynamically unstable species on porous materials provides a significant enthalpy stabilization of the adsorbates.[50] The change in the thermodynamic state of the Ti(BH$_4$)$_3$ molecule opens the possibility for a new decomposition reaction pathway. The lack of diborane emission is evidence of a modification in the decomposition pathway of the adsorbed molecule. The spectroscopic evidence suggests a decomposition reaction pathway that involves pentaborane as an intermediate step:

$$2Ti(BH_4)_3 \rightarrow 2TiH_3 + B_5H_9 + B + 9/2H_2$$
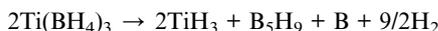
and where the pentaborane recombines at the increased temperature to form solid higher boranes. Modification of decomposition reaction pathways has already been observed for melt infiltrated complex hydrides in nanoporous materials and has been attributed to effects due to the confinement of the complex hydride in the pores.[51,52] The different decomposition mechanism might indicate reversible hydrogen sorption reactions of Ti(BH$_4$)$_3$. Previous studies identified diborane as one of the key elements restricting this process. Therefore, this new system might be reversible due to the lack of diborane emission.[13] These findings open up new opportunities for the thorough investigation of the effects of surfaces on adsorbents.

Conclusions

Ti(BH$_4$)$_3$, a highly reactive gaseous molecule at room temperature, was incorporated into a metal–organic framework and found to be thermodynamically stabilized. The adsorption on a MOF stabilizes unstable Ti(BH$_4$)$_3$ for months and changes the energy configuration of the system. The adsorption is achieved without reaction with the scaffold matrix and is potentially reversible. This new approach allows for the safe storage and easy handling of volatile unstable complex hydrides. Additionally, it provides an opportunity for the physical characterization of transient states. The lack of chemical bonding or substitution between the transient species and the framework allows for the release of the species upon heating or air exposure and allows for subsequent guest reloading in the framework.

This case study opens a new route for the practical use of a class of transient materials that is interesting for energy storage and, more generally, acts as a proof of concept of the stabilization of rapidly evolving species.

Acknowledgements

References

1 *Chemical Energy Storage*, ed. Robert Schlögl, Walter de Gruyter, 2012.

2 *Hydrogen as a Future Energy Carrier*, ed. A. Züttel, A. Borgschulte and L. Schlapbach, Wiley-VCH Verlag GmbH & Co. KGaA, 2008.

3 *Hydrogen Storage Technology: Materials and Applications*, ed. L. Klebanoff, CRC Press, Boca Raton, 1st edn, 2012.

4 B. Sakintuna, F. Lamari-Darkrim and M. Hirscher, *Int. J. Hydrogen Energy*, 2007, **32**, 1121–1140.

5 M. Paskevicius, D. A. Sheppard and C. E. Buckley, *J. Am. Chem. Soc.*, 2010, **132**, 5077–5083.

6 P. Mauron, F. Buchter, O. Friedrichs, A. Remhof, M. Bielmann, C. N. Zwicky and A. Züttel, *J. Phys. Chem. B*, 2008, **112**, 906–910.

7 A. Borgschulte, R. Gremaud, Z. Łodziana and A. Züttel, *Phys. Chem. Chem. Phys.*, 2010, **12**, 5061–5066.

8 M. Chong, A. Karkamkar, T. Autrey, S. Orimo, S. Jalisatgi and C. M. Jensen, *Chem. Commun.*, 2011, **47**, 1330–1332.

9 N. P. Stadie, E. Callini, B. Richter, T. R. Jensen, A. Borgschulte and A. Züttel, *J. Am. Chem. Soc.*, 2014, **136**, 8181–8184.

10 A. F. Dalebrook, W. Gan, M. Grasemann, S. Moret and G. Laurenczy, *Chem. Commun.*, 2013, **49**, 8735–8751.

11 D. J. Durbin and C. Malardier-Jugroot, *Int. J. Hydrogen Energy*, 2013, **38**, 14595–14617.

12 K. Miwa, N. Ohba, S. Towata, Y. Nakamori, A. Züttel and S. Orimo, *J. Alloys Compd.*, 2007, **446–447**, 310–314.

13 E. Callini, A. Borgschulte, C. L. Hugelshofer, A. J. Ramirez-Cuesta and A. Züttel, *J. Phys. Chem. C*, 2014, **118**, 77–84.

14 H. R. Hoekstra and J. J. Katz, *J. Am. Chem. Soc.*, 1949, **71**, 2488.

15 H. I. Schlesinger, R. T. Sanderson and A. B. Burg, *J. Am. Chem. Soc.*, 1940, **62**, 3421–3425.

16 R. Matsuda, R. Kitaura, S. Kitagawa, Y. Kubota, R. V. Belosludov, T. C. Kobayashi, H. Sakamoto, T. Chiba, M. Takata, Y. Kawazoe and Y. Mita, *Nature*, 2005, **436**, 238–241.

17 D. A. Knight, R. Zidan, R. Lascola, R. Mohtadi, C. Ling, P. Sivasubramanian, J. A. Kaduk, S.-J. Hwang, D. Samanta and P. Jena, *J. Phys. Chem. C*, 2013, **117**, 19905–19915.

18 Y. Guo, X. Yu, W. Sun, D. Sun and W. Yang, *Angew. Chem., Int. Ed.*, 2011, **50**, 1087–1091.

19 P. Sivasubramanian, R. Mohtadi, R. Zidan, K. Pariyadath, C. L. Leverette and M. L. Fetterolf, *Appl. Spectrosc.*, 2012, **66**, 591–594.

20 S. Gudmundsdóttir, E. Skúlason, K.-J. Weststrate, L. Juurlink and H. Jónsson, *Phys. Chem. Chem. Phys.*, 2013, **15**, 6323–6332.

21 K. Tedsree, T. Li, S. Jones, C. W. A. Chan, K. M. K. Yu, P. A. J. Bagot, E. A. Marquis, G. D. W. Smith and S. C. E. Tsang, *Nat. Nanotechnol.*, 2011, **6**, 302–307.

22 W. J. Durand, A. A. Peterson, F. Studt, F. Abild-Pedersen and J. K. Nørskov, *Surf. Sci.*, 2011, **605**, 1354–1359.

23 A. A. Peterson and J. K. Nørskov, *J. Phys. Chem. Lett.*, 2012, **3**, 251–258.

24 J. F. Hull, Y. Himeda, W.-H. Wang, B. Hashiguchi, R. Periana, D. J. Szalda, J. T. Muckerman and E. Fujita, *Nat. Chem.*, 2012, **4**, 383–388.

25 L. Valenzano, B. Civalleri, S. Chavan, S. Bordiga, M. H. Nilsen, S. Jakobsen, K. P. Lillerud and C. Lamberti, *Chem. Mater.*, 2011, **23**, 1700–1718.

26 M. J. Katz, Z. J. Brown, Y. J. Colón, P. W. Siu, K. A. Scheidt, R. Q. Snurr, J. T. Hupp and O. K. Farha, *Chem. Commun.*, 2013, **49**, 9449–9451.

27 J. H. Cavka, S. Jakobsen, U. Olsbye, N. Guillou, C. Lamberti, S. Bordiga and K. P. Lillerud, *J. Am. Chem. Soc.*, 2008, **130**, 13850–13851.

28 L. J. Murray, M. Dincă and J. R. Long, *Chem. Soc. Rev.*, 2009, **38**, 1294–1314.

29 L. Li, S. Tang, C. Wang, X. Lv, M. Jiang, H. Wu and X. Zhao, *Chem. Commun.*, 2014, **50**, 2304–2307.

30 D. F. Sava, M. A. Rodriguez, K. W. Chapman, P. J. Chupas, J. A. Greathouse, P. S. Crozier and T. M. Nenoff, *J. Am. Chem. Soc.*, 2011, **133**, 12398–12401.

31 C. Hon Lau, R. Babarao and M. R. Hill, *Chem. Commun.*, 2013, **49**, 3634–3636.

32 G. Li, H. Kobayashi, J. M. Taylor, R. Ikeda, Y. Kubota, K. Kato, M. Takata, T. Yamamoto, S. Toh, S. Matsumura and H. Kitagawa, *Nat. Mater.*, 2014, **13**, 802–806.

33 J. Park, D. Yuan, K. T. Pham, J.-R. Li, A. Yakovenko and H.-C. Zhou, *J. Am. Chem. Soc.*, 2012, **134**, 99–102.

34 Y. Huang, W. Qin, Z. Li and Y. Li, *Dalton Trans.*, 2012, **41**, 9283–9285.

35 H. Sato, W. Kosaka, R. Matsuda, A. Hori, Y. Hijikata, R. V. Belosludov, S. Sakaki, M. Takata and S. Kitagawa, *Science*, 2014, **343**, 167–170.

36 L. Chen, P. S. Reiss, S. Y. Chong, D. Holden, K. E. Jelfs, T. Hasell, M. A. Little, A. Kewley, M. E. Briggs, A. Stephenson, K. M. Thomas, J. A. Armstrong, J. Bell, J. Busto, R. Noel, J. Liu, D. M. Strachan, P. K. Thallapally and A. I. Cooper, *Nat. Mater.*, 2014, **13**, 954–960.

37 J.-R. Li, J. Yu, W. Lu, L.-B. Sun, J. Sculley, P. B. Balbuena and H.-C. Zhou, *Nat. Commun.*, 2013, **4**, 1538.

38 A. de Juan and R. Tauler, *Crit. Rev. Anal. Chem.*, 2006, **36**, 163–176.

39 J. Jaumot, R. Gargallo, A. de Juan and R. Tauler, *Chemom. Intell. Lab. Syst.*, 2005, **76**, 101–110.

40 E. P. Barrett, L. G. Joyner and P. P. Halenda, *J. Am. Chem. Soc.*, 1951, **73**, 373–380.

41 Y. Nakamori, K. Miwa, A. Ninomiya, H. Li, N. Ohba, S. Towata, A. Züttel and S. Orimo, *Phys. Rev. B: Condens. Matter Mater. Phys.*, 2006, **74**, 045126.

42 G. Sokrates, *Infrared and Raman Characteristic Group Frequencies: Tables and Charts*, John Wiley & Sons, 3rd edn, 2004.

43 M. Kandiah, M. H. Nilsen, S. Usseglio, S. Jakobsen, U. Olsbye, M. Tilset, C. Larabi, E. A. Quadrelli, F. Bonino and K. P. Lillerud, *Chem. Mater.*, 2010, **22**, 6632–6640.

44 L. Maschio, B. Kirtman, M. Rérat, R. Orlando and R. Dovesi, *J. Chem. Phys.*, 2013, **139**, 164101.

45 E. Callini, A. Borgschulte, A. J. Ramirez-Cuesta and A. Züttel, *Dalton Trans.*, 2013, **42**, 719–725.

46 C. J. Dain, A. J. Downs and D. W. H. Rankin, *Angew. Chem., Int. Ed. Engl.*, 1982, **21**, 534–535.

47 C. J. Dain, A. J. Downs, M. J. Goode, D. G. Evans, K. T. Nicholls, D. W. H. Rankin and H. E. Robertson, *J. Chem. Soc., Dalton Trans.*, 1991, 967–977.

48 C. Lamberti, A. Zecchina, E. Groppo and S. Bordiga, *Chem. Soc. Rev.*, 2010, **39**, 4951–5001.

49 M. Moskovits and J. S. Suh, *J. Phys. Chem.*, 1984, **88**, 5526–5530.

50 N. Artioli, R. F. Lobo and E. Iglesia, *J. Phys. Chem. C*, 2013, **117**, 20666–20674.

51 A. Remhof, P. Mauron, A. Züttel, J. P. Embs, Z. Łodziana, A. J. Ramirez-Cuesta, P. Ngene and P. de Jongh, *J. Phys. Chem. C*, 2013, **117**, 3789–3798.

52 J. Gao, P. Adelhelm, M. H. W. Verkuijlen, C. Rongeat, M. Herrich, P. J. M. van Bentum, O. Gutfleisch, A. P. M. Kentgens, K. P. de Jong and P. E. de Jongh, *J. Phys. Chem. C*, 2010, **114**, 4675–4682.